Spatial Analysis of 3′ Phosphoinositide Signaling in Living Fibroblasts: I. Uniform Stimulation Model and Bounds on Dimensionless Groups

Jason M. Haugh and Ian C. Schneider
Department of Chemical Engineering, North Carolina State University, Raleigh, North Carolina 27695

ABSTRACT Fluorescent protein probes now permit spatial distributions of specific intracellular signaling molecules to be observed in real time. Mathematical models have been used to simulate molecular gradients and other spatial patterns within cells, and the output of such models may be compared directly with experiments if the binding of the fluorescent probe and the physics of the imaging technique are each incorporated. Here we present a comprehensive model describing the dynamics of 3′ phosphoinositides (PIs), lipid second messengers produced in the plasma membrane in response to stimulation of the PI 3-kinase signaling pathway, as monitored in the cell-substratum contact area using total internal reflection fluorescence microscopy. With this technique it was previously shown that uniform stimulation of fibroblasts with platelet-derived growth factor elicits the formation of axisymmetric 3′ PI gradients, which we now characterize in the context of our model. We find that upper and lower bounds on the relevant dimensionless model parameter values for an individual cell can be calculated from four well-defined fluorescence measurements. Based on our analysis, we expect that the key dimensionless group, the ratio of 3′ PI turnover and diffusion rates, can be estimated within ~20% or less.

INTRODUCTION

Cells in multicellular organisms must coexist, and thus their behaviors are tightly regulated through inter- and intracellular signaling mechanisms. Although our knowledge of the complex biochemical interactions used by cells to process information has rapidly expanded (Hunter, 2000), the integration of these molecular-level details into a holistic framework is now presenting a significant challenge. A tool that has shown promise in the synthesis and analysis of signal transduction networks is mathematical modeling (Weng et al., 1999; Asthagiri and Lauffenburger, 2000). Most of the signaling models offered to date have been of the kinetic variety, comprised of deterministic, ordinary differential equations in which the amounts of molecular species in various states change with respect to time only. Such models are appropriate for comparison with cell biochemical experiments, in which a large number of cells are homogenized and analyzed. Although these methods can be quantitative and are appropriate for determining population averages, it must be acknowledged that the concentrations of signaling components vary from cell to cell, and that the kinetics of individual cell responses may be asynchronous and/or noisy.

Another aspect of cell signaling that is not adequately addressed in either ordinary differential equation kinetic models or cell biochemical experiments is the spatial distribution of the intracellular species. Although kinetic models can effectively model exchange of signaling molecules between intracellular locations and compartments (Haugh and Lauffenburger, 1998; Xu et al., 2003), that approach does not lend itself to the description of spatial gradients in molecular concentration, which can form through production of molecules at localized intracellular sites. In such cases, partial differential equations can be formulated in spatial dimensions as well as time, and thus molecular transport mechanisms can be modeled explicitly. Computational approaches for the efficient simulation of three-dimensional spatial patterns within the cytosol have been conceived and used to compare models with spatially resolved fluorescence imaging experiments (Schaff et al., 1997; Fink et al., 1999).

Two-dimensional molecular gradients in cell membranes are also relevant in signal transduction. Most signaling pathways involve specific membrane-associated intermediates that are produced or activated through recruitment of signaling enzymes to the plasma membrane. Gradients in the density of specific membrane lipids or activated lipid-anchored proteins may form on the nanometer scale if the rates of the reactions that produce them are rapid enough to be limited by lateral diffusion (Shea et al., 1997; Haugh, 2002), and gradients on longer length scales can form when the extracellular stimulus is spatially confined or otherwise organized. A prominent example is the production of 3′ phosphoinositide (PI) lipids through activation of the intracellular enzyme PI 3-kinase (Vanhaesebroeck et al., 2001). One of the cellular functions of 3′ PI lipids is to influence cell adhesion, spreading, and motility through remodeling of the actin cytoskeleton (Rameh and Cantley, 1999), and thus the localization of 3′ PI production is critical for cell guidance (Weiner, 2002). Localization can be induced by gradients of soluble factors or extracellular matrix components, or by cellular interactions with other cells or particles, and such systems lend themselves to partial differential equation modeling (Narang et al., 2001; Postma and Van Haastert, 2001; Levchenko and Iglesias, 2002; Pribyl et al., 2003) and fluorescence microscopy techniques (Parent and Devreotes, 1999; Botelho et al., 2000; Marshall

Submitted July 15, 2003, and accepted for publication September 23, 2003.

Address reprint requests to Jason M. Haugh, Box 7905, North Carolina State University, Raleigh, NC 27695. Tel.: 919-513-3851; Fax: 919-515-3465; E-mail: jason_haugh@ncsu.edu.

0006-3495/04/01/589/10 $2.00

et al., 2001; Harriague and Bismuth, 2002; Wang et al., 2002). However, no studies have yet successfully integrated modeling and experiments of lipid second messenger signaling, to the extent of a quantitative and direct comparison with respect to space as well as time.

Even when cell stimulation is spatially uniform, intracellular gradients can form if activation of cell surface receptors is confined to certain regions of the plasma membrane. Indeed, in previous work using an enhanced green fluorescent protein fusion probe (GFP-AktPH) and high-resolution total internal reflection fluorescence (TIRF) microscopy, it was found that two kinds of 3′ PI lipid gradients can form in the membrane-substratum contact area of platelet-derived growth factor (PDGF)-stimulated fibroblasts. In the presence of a PDGF gradient, 3′ PI production is polarized toward the highest PDGF concentration, whereas uniform PDGF stimulation yields a radial 3′ PI gradient, presumably through the restriction of PDGF-stimulated PI 3-kinase activation to the nonadherent portion of the membrane (Haugh et al., 2000). In either case, the ability to maintain a second messenger gradient within a cell of given dimensions depends on the relative rates of turnover, mediated by specific enzymatic activities, and molecular transport, typically dominated by diffusion.

In this work, we present a generalized mathematical model that describes the 3′ PI dynamics in response to uniform stimulation. With appropriate assumptions, it is shown that the model can directly simulate TIRF intensity measurements in fibroblasts, and that the prominent features of these simulations are sensitive to the values of the dimensionless model parameters. Although the fluorescence characteristics of a cell do not correspond to a unique set of parameter values, upper and lower bounds on each of the parameters are defined by examining specific limiting cases of the model. Using this constraints-based approach, we demonstrate that the primary parameter of interest, which compares the rates of 3′ PI turnover and diffusion, can be estimated with reasonable precision from defined fluorescence measurements.

GENERALIZED UNIFORM STIMULATION MODEL

Axisymmetric reaction-diffusion model of 3′ phosphoinositide dynamics

The geometry of the model cell is depicted in Fig. 1. In this formulation of the model, the hemispherical top and circular bottom membrane domains of the model cell are allowed to have different rates of 3′ PI generation, diffusion in two dimensions, and consumption by first-order reaction(s) (Fig. 1 *a*). The generalized conservation equation for the 3′ PI number density X (molecules/μm^2) in each domain i (bottom or top) is thus

$$\partial X_i/\partial t = D_i\nabla^2 X_i - k_i X_i + V_i(t), \qquad (1)$$

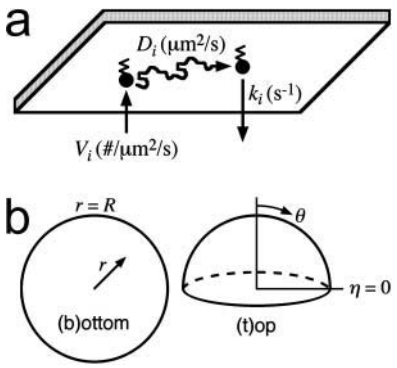

FIGURE 1 Generalized lipid second messenger model. (*a*) Within each membrane domain i, the lipid second messenger is inserted at random positions at a rate V_i. Once inserted, the lipid experiences lateral diffusion with effective diffusion coefficient D_i, and it is consumed with observed first-order rate constant k_i. (*b*) Geometry and spatial coordinates of the two domains.

where t is time, D_i is the molecular diffusion coefficient, k_i the observed consumption rate constant, and $V_i(t)$ the generation rate of the second messenger in domain i. The kinetics of the latter depend on the assembly of ligand, receptor, and intracellular enzyme molecules. The symmetry of the problem is such that the 3′ PI distribution in the bottom domain varies with radial position r only, and that of the top domain varies with azimuthal angle θ only ($\eta = \cos\theta$) (Fig. 1 *b*). The interface joining the two domains ($r = R$ and $\eta = 0$) is subject to matching boundary conditions:

$$X_b(R,t) = X_t(0,t)$$
$$D_b\nabla X_b(R,t) = D_t\nabla X_t(0,t). \qquad (2)$$

Additionally, $X_b(r,t)$ and $X_t(\eta,t)$ must be finite. Our solution employs the following dimensionless variables and parameters:

$$x_i \equiv \frac{X_i}{X^*};\quad \tau \equiv k_b t;\quad \rho \equiv \frac{r}{R};\quad \upsilon_i(\tau) \equiv \frac{V_i(t)}{k_i X^*};$$
$$Da = \frac{k_b R^2}{D_b};\quad \alpha \equiv \frac{k_t}{k_b};\quad \gamma \equiv \frac{D_t}{D_b};\quad \nu \equiv \frac{V_{t,ss}k_b}{V_{b,ss}k_t}, \qquad (3)$$

where X^* is, for now, an arbitrary scaling quantity in units of number density, and $V_{t,ss}$ and $V_{b,ss}$ are the steady-state values of $V_t(t)$ and $V_b(t)$, respectively. Perhaps the most important of the model parameters is the Damköhler number Da, which compares the rates of 3′ PI consumption and diffusion in the bottom domain and thus controls the formation of 3′ PI gradients there. The details of the solution and the calculation of $x_b(\rho,\tau)$ and $x_t(\eta,\tau)$ are given in Appendix A.

TIRF intensity profiles and simulation of association-dissociation experiments

A model of the 3′ PI dynamics is not sufficient for comparison with experiments, because the spatial distribution

of specific membrane lipids cannot be measured directly. Rather, the most common method is to use an intracellular fluorescent probe that binds specifically to 3′ PIs, such as GFP-AktPH, which will translocate from the cytosol to the plasma membrane as the 3′ PI level increases. The extent of probe translocation is then resolved by fluorescence microscopy, and thus the nature of the fluorescence intensity data depends on the imaging technique used. We focus our attention on the aforementioned TIRF microscopy technique, in which an evanescent wave selectively excites intracellular fluorophores in close proximity to the membrane-substratum contact area (Axelrod, 2001; Steyer and Almers, 2001; Toomre and Manstein, 2001). The fluorescence intensity is thus a sum of contributions from membrane-bound probe and a small fraction of the unbound, cytosolic probe molecules.

We assume that the binding of a fluorescent probe to the membrane is in pseudo-equilibrium with free probe in the cytosol. Based on experiments in a macrophage cell line, it has been determined that it requires ~5 s for membrane-bound GFP-AktPH probe to exchange with the cytosolic pool (Marshall et al., 2001), significantly faster than the timescale of 3′ PI turnover in fibroblasts or macrophages, ~1 min (Haugh et al., 2000; Marshall et al., 2001). Distribution of GFP-AktPH within the cytosol is assumed to be similarly rapid, based on an intracellular diffusion coefficient for enhanced GFP of ~40 $\mu m^2/s$ (Yokoe and Meyer, 1996; Swaminathan et al., 1997) and a characteristic length scale of 10 μm. The normalized fluorescence intensity for TIRF excitation, $f(\rho,\tau)$, is then readily calculated from the 3′ PI distributions, as described in Appendix B. Importantly, this quantity can be determined from fluorescence image data, allowing a direct comparison of model and experiment. To obtain $f(\rho,\tau)$, three dimensionless groups must be specified in addition to those listed in Eq. 3:

$$\sigma \equiv \frac{V_{cyt}}{A_c d_{cell}}; \quad \kappa \equiv \frac{K_D V_{cyt}}{P_{Tot}}; \quad \mu \equiv \frac{A_c X^*}{P_{Tot}}, \tag{4}$$

where V_{cyt} is the volume of the cytosol, A_c is the cell contact area ($A_c = \pi R^2$ for our model cell), d_{cell} is the effective penetration depth of the evanescent wave into the cell (~100 nm), K_D is the dissociation constant of the probe-3′ PI interaction, and P_{Tot} is the total number of probe molecules in the cell. The fluorescence gain parameter σ is the fold increase in evanescent wave fluorescence observed when a probe molecule translocates from the cytosol to the contact area, and thus it is the only parameter that reflects the physics of the imaging technique. The other two parameters, along with the calculated number of 3′ PI molecules in the cell, determine the extent of probe-3′ PI binding. The fraction of the probe recruited to the plasma membrane is defined as $p(\tau)$, and its value at steady state, p_{ss}, can be specified in place of either κ or μ. The dimensionless model variables and parameters are summarized in Table 1.

TABLE 1 Dimensionless variables and parameters

Variable	Definition	Description
ρ	r/R	Dimensionless radius, bottom domain
τ	$k_b t$	Dimensionless time
$x_b(\rho,\tau)$	$X_b(r,t)/X^*$	Lipid number density, bottom domain
$x_t(\eta,\tau)$	$X_t(\eta,t)/X^*$	Lipid number density, top domain
$f(\rho,\tau)$	$F(r,t)/F_{cyt}-1$	Dimensionless fluorescence intensity
$p(\tau)$		Fraction of fluorescent probe bound
Parameter	**Definition**	**Description**
Da	$k_b R^2/D_b$	Damköhler No.; consumption versus diffusion
α	k_t/k_b	Ratio of lipid consumption rate constants
γ	D_t/D_b	Ratio of lipid diffusion coefficients
ν	$V_{b,ss}k_t/V_{t,ss}k_b$	Ratio of steady-state lipid insertion rates
σ	$V_{cyt}/A_c d_{cell}$	Fluorescence gain parameter
κ	$K_D V_{cyt}/P_{Tot}$	Dimensionless probe dissociation constant
μ	$A_c X^*/P_{Tot}$	Maximum ratio of lipid/probe molecules
x_0	$x_b(\rho,0)$	Pre-stimulus lipid density (constant)

We have designed an experimental TIRF microscopy protocol to examine the accumulation of 3′ PIs in the contact area during stimulation with PDGF, and the subsequent decay of the 3′ PI level after the addition of a PI 3-kinase inhibitor. These are termed association-dissociation experiments because of the net changes in the membrane recruitment of the GFP-AktPH probe induced by the two treatments. Here we wish to use the uniform stimulation model to simulate these experiments, as illustrated in Fig. 2. To visualize the kinetics of GFP-AktPH recruitment as well as the development of a radial 3′ PI gradient, three normalized fluorescence values are followed with time: the values at the center and periphery of the contact area ($f(0,\tau)$ and $f(1,\tau)$, respectively), and the value averaged over the surface of the contact area ($\bar{f}(\tau)$) (Fig. 2 *b*). Although the model can accommodate any kinetics for the stimulation of PI 3-kinase activity, for simplicity we assume step changes ($\upsilon_t(\tau) = 1$, $\upsilon_b(\tau) = \nu$ for association, $\upsilon_t(\tau) = \upsilon_b(\tau) = 0$ for dissociation; Appendix A). In the companion article that follows, this assumption is validated for our cells when the concentrations of PDGF and inhibitor are sufficiently high.

RESULTS

The steady-state fluorescence profile and aspects of the simulated probe association kinetics are sensitive to the relative rates of 3′ PI consumption and diffusion

As described in the previous section, the uniform stimulation model can be used to simulate association-dissociation experiments; the simplest and most general aspect of these simulations is the steady-state fluorescence profile, $f_{ss}(\rho)$. Two useful metrics that characterize this profile are the ratio of the net fluorescence intensity at the center of the contact area relative to the average, $f_{ss}(0)/\bar{f}_{ss}$, and the average fluorescence normalized by the extent of probe binding, $\bar{f}_{ss}/p_{ss}$.

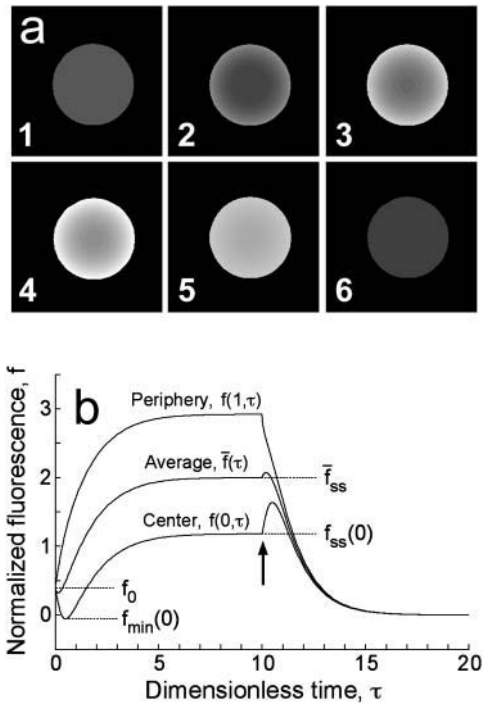

FIGURE 2 Simulation of association-dissociation fluorescence experiments. Calculations are shown for a simulated cell contact area imaged with total internal reflection fluorescence excitation. Dimensionless parameters are $Da = 3$, $\alpha = \gamma = 1$, $\nu = 0$, $p_{ss} = 0.75$, $\kappa = 0.3$, $\sigma = 16.8$, and $x_0 = 0.047$. (*a*) Panel *1* shows the simulated cell before treatment, and panels *2*, *3*, and *4* show the contact area at $\tau = 0.5$, 2, and 10 after addition of PDGF, simulated as a step increase in the 3′ PI production rate in the top domain (association phase). The 3′ PI production is then inhibited abruptly at $\tau = 10$, and the fluorescence decays (dissociation phase); panels *5* and *6* show the contact area at $\tau = 10.6$ and 20. (*b*) The simulated profiles at all time points were converted into kinetic traces by plotting the normalized fluorescence intensities at the contact area periphery $f(1,\tau)$, at the contact area center $f(0,\tau)$, and averaged over the contact area $\bar{f}(\tau)$. Time zero corresponds to the addition of PDGF, and the arrow signifies the inhibition of PI 3-kinase activity. Also indicated on the plot are the initial fluorescence (f_0), the minimum fluorescence achieved at the contact area center ($f_{min}(0)$), and the steady-state fluorescence values at the center ($f_{ss}(0)$) and averaged over the contact area ($\bar{f}_{ss}$).

Analytical expressions for these quantities are given in Appendix A, and our analysis of these equations is shown in Fig. 3, *a* and *b*.

With base parameter assumptions ($\alpha = \gamma = 1$, $\nu = 0$; Fig. 3 *a*), the steady-state fluorescence profile is determined by *Da*, the Damköhler number that compares the rates of lipid consumption and diffusion, and σ, the fluorescence gain parameter. Hence, from given values of $f_{ss}(0)$ and $\bar{f}_{ss}$, conservative upper and lower limits on the value of *Da* are imposed. The maximum *Da* is given by the value of $f_{ss}(0)/\bar{f}_{ss}$ in the limit of very large σ, whereas the minimum value is set by $\bar{f}_{ss}/p_{ss} = \bar{f}_{ss}$. For example, consider a cell with $f_{ss}(0)/\bar{f}_{ss} = 0.60$ and $\bar{f}_{ss} = 2.0$. With base parameter assumptions, the range of possible *Da* values is from 2.61 to 4.43, and the lower limit on σ is 13.2. Varying the parameters α, γ, and ν, which relate the consumption rate constants, diffusion coefficients, and steady-state generation rates in the two domains, respectively, shifts the $f_{ss}(0)/\bar{f}_{ss}$ and $\bar{f}_{ss}/p_{ss}$ curves (Fig. 3 *b*). Most significantly, increasing ν requires a higher value of *Da* to achieve the same fluorescence profile, whereas the corresponding value of σ changes very little. Variation of γ, the dimensionless diffusion coefficient in the top domain, has the opposite effect: the required value of *Da* changes little, whereas the value of σ decreases as γ increases. In other words, enhancing the 3′ PI flux from the top of the cell into the contact area can be offset simply by decreasing the fluorescence gain σ. Reducing the consumption rate constant in the top membrane domain, by lowering α, has the same effect (not shown).

Additional insights are gained through an analysis of the simulated association kinetics in response to a large dose of PDGF. As depicted in Fig. 2, the most compelling feature of the kinetics is a dip in the fluorescence at the center of the contact area, $f_{min}(0)$, caused at least in part by the recruitment of probe molecules from the cytosol to the top of the cell. Thus, the fluorescence dip should be sensitive to the rate at which the 3′ PIs are distributed between the two membrane domains, determined in the model by the value of *Da*. In Fig. 3 *c*, probe association was simulated with base parameters ($\alpha = \gamma = 1$, $\nu = 0$), and as *Da* was varied, the gain parameter σ and the basal lipid density x_0 were adjusted so that the initial fluorescence, f_0, and the average fluorescence at steady state, $\bar{f}_{ss}$, would be set to the same values of 0.4 and 2.0, respectively. In addition to affecting the steady-state profile (as predicted from Fig. 3 *a*), increasing the value of *Da* also affects the initial dip at the center of the contact area. As the rate of lipid diffusion is effectively reduced, lower values of $f_{min}(0)$ are achieved, and the minimum fluorescence occurs at later times.

Kinetic analyses varying the parameters α and γ: what can we say about the top of the cell?

The dimensionless constants α and γ are ratios of the consumption rate constants and diffusion coefficients in the two domains, respectively ($\alpha \equiv k_t/k_b$; $\gamma \equiv D_t/D_b$). Deviation from the base assumptions ($\alpha = \gamma = 1$) would thus accommodate spatially regulated lipid consumption activities or a reduced molecular mobility in the adherent contact area. As shown in the steady-state analysis (Fig. 3 *b*), these parameters affect the lipid flux from the top to the bottom of the cell, which influences the magnitude of the steady-state 3′ PI profile $x_{b,ss}(\rho)$ but not its shape; i.e., the same steady-state fluorescence profile $f_{ss}(\rho)$ can be attained by adjusting the gain parameter σ. However, variation of these parameters may also affect the association and/or dissociation kinetics; indeed, at least for α, it would be surprising if this were not so.

Dissociation experiments focus on the kinetics of 3′ PI consumption. Analysis of the model equations indicates that, during dissociation with $\alpha < 1$, the center/average ratio

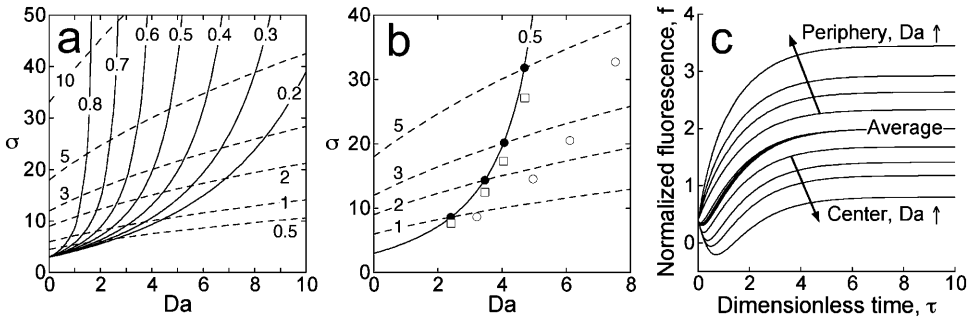

FIGURE 3 Effect of 3′ PI diffusion on simulated association kinetics. (*a* and *b*) Steady-state analysis. The curves map the values of the Damköhler number Da and gain parameter σ that yield the indicated steady-state values of the minimum/average ratio $f_{ss}(0)/\bar{f}_{ss}$ (*solid lines*) and average fluorescence/probe binding ratio $\bar{f}_{ss}/p_{ss}$ (*dashed lines*), according to Eqs. A9 and A10, respectively (Appendix A). (*a*) Base-case parameters: $\alpha = \gamma = 1$, $\nu = 0$. (*b*) Closed circles mark the intersections of $f_{ss}(0)/\bar{f}_{ss}$ and $\bar{f}_{ss}/p_{ss}$ curves for base-case parameters; the open circles are the corresponding positions with $\alpha = \gamma = 1$, $\nu = 0.1$, and the open squares are the positions with $\alpha = 1$, $\gamma = 3$, $\nu = 0$. (*c*) Simulated association experiments. The following parameters were used: $\alpha = \gamma = 1$, $\nu = 0$, $p_{ss} = 0.75$, and $\kappa = 0.3$. As Da was varied, the values of σ and x_0 were adjusted to maintain $f_0 = 0.4$ and $\bar{f}_{ss} = 2.0$, as in Fig. 2. Values of Da (σ, x_0) are 1 (13.2, 0.064), 2 (15.1, 0.053), 3 (16.8, 0.047), and 5 (19.9, 0.038).

$f_{ss}(0)/\bar{f}_{ss}$ should approach a pseudo steady-state value that is also <1. This is confirmed in Fig. 4,*a* and *b*. When $\alpha < 1$, the center, average, and periphery fluorescence curves clearly do not converge (Fig. 4 *a*), and $f_{ss}(0)/\bar{f}_{ss}$ does not approach unity (Fig. 4 *b*). We conclude that the assumption $\alpha = 1$ can be accepted when fluorescence profiles consistently become homogeneous during the dissociation time course. Varying γ, on the other hand, does not significantly alter the kinetics of association or dissociation once the σ and x_0 values are adjusted to match the values of f_0 and $\bar{f}_{ss}$ (Fig. 4 *c* and results not shown). Therefore, the model is not uniquely sensitive to and cannot be used to evaluate D_t. It is heartening, however, that the variation of γ by as much as a factor of 3 affects the estimation of σ and x_0 only modestly and does not influence the estimation of the other parameters. Based on the considerations above, we will assume that both α and γ are equal to 1 for the remainder of this work.

The dip in fluorescence at the center of the contact area is sensitive to characteristics of the intracellular probe

Motivated by the prominence of the transient dip in fluorescence at the center of the contact area, $f_{min}(0)$, a full parametric analysis of this metric was performed. As in the previous sections, the parameters were adjusted to achieve the same values of f_0 and $\bar{f}_{ss}$ (0.40 and 2.00, respectively); the value of $f_{ss}(0)$ was also set here to 1.18, the value obtained with $Da = 3$ in Figs. 2–4. Two assumptions regarding the PI 3-kinase activity in the contact area were examined, corresponding to its disappearance or maintenance of the basal activity ($\nu = 0$ or $\nu = x_0$, respectively). With these constraints, and assuming $\alpha = \gamma = 1$, the specification of any two model parameters, among Da, σ, x_0, p_{ss}, and κ (μ can be substituted for either p_{ss} or κ), yields the values of the remaining three. With all of the dimensionless parameters in hand, the value of $f_{min}(0)$ follows.

The dependence of $f_{min}(0)$ on the extent of probe binding p_{ss} with various values of κ, μ, or x_0 is shown in Fig. 5, yielding a number of conclusions. As expected, lower $f_{min}(0)$ values are achieved when more of the probe is recruited from the cytosol (higher p_{ss}). For a given value of p_{ss}, lower $f_{min}(0)$ values are achieved with higher κ; with the extent of binding fixed and a lower probe affinity, the 3′ PI lipids must increasingly outnumber probe molecules, allowing more of the probe to be recruited to the top of the cell before diffusion can redistribute the lipid (also seen with higher μ). Also, comparison of Fig. 5, *a* and *b*, shows that a significantly

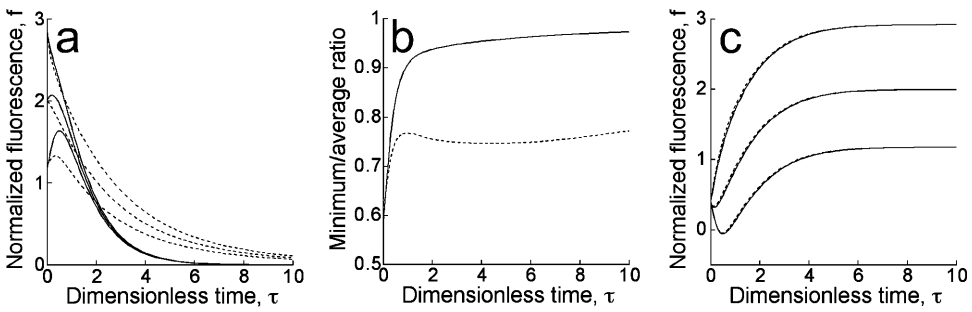

FIGURE 4 Consumption and diffusion of 3′ PIs in the top and bottom domains. Unless otherwise noted, the following parameters were used: $Da = 3$, $\alpha = \gamma = 1$, $\nu = 0$, $p_{ss} = 0.75$, and $\kappa = 0.3$. The values of σ and x_0 were adjusted to maintain $f_0 = 0.4$ and $\bar{f}_{ss} = 2.0$, as in Figs. 2 and 3. (*a*) Calculated dissociation time courses with $\alpha = 1$, $\sigma = 16.8$ (*solid lines*), or $\alpha = 0.3$, $\sigma = 20.0$ (*dashed lines*). (*b*) The minimum/average ratio, calculated from the data in *a*, does not approach unity when $\alpha \neq 1$. (*c*) Calculated association time courses with $\gamma = 1$, $\sigma = 16.8$, $x_0 = 0.047$ (*solid lines*), or $\gamma = 3$, $\sigma = 14.7$, $x_0 = 0.055$ (*dashed lines*).

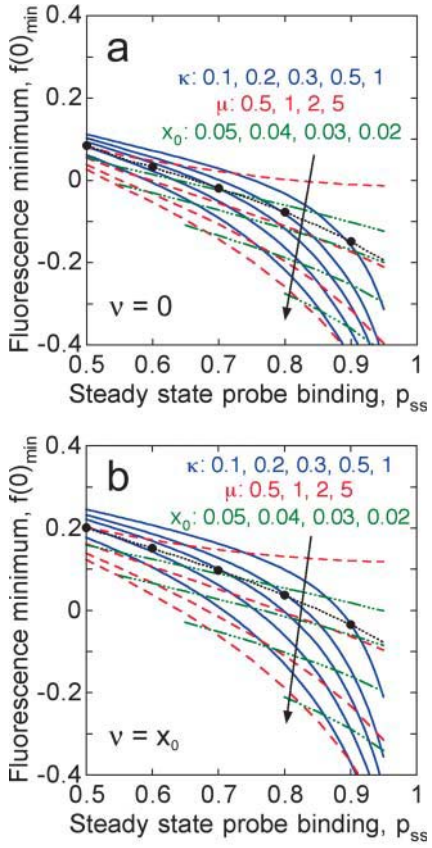

FIGURE 5 Parametric analysis of the dip in center fluorescence. The minimum fluorescence at the center of the contact area, $f_{min}(0)$, was calculated for various values of p_{ss} with $\nu = 0$ (*a*) or $\nu = x_0$ (*b*), and other parameters chosen to maintain $f_0 = 0.40$, $\bar{f}_{ss} = 2.00$, and $f_{ss}(0) = 1.18$. Curves are for constant values of κ (0.1, 0.2, 0.3, 0.5, or 1; *blue*), μ (0.5, 1, 2, or 5; *red*), or x_0 (0.02, 0.03, 0.04, or 0.05; *green*). The black curves satisfy $\kappa = 1 - p_{ss}$.

lower value of $f_{min}(0)$ is achieved when the basal PI 3-kinase activity disappears from the contact area ($\nu = 0$). The sudden loss of PI 3-kinase activity from the bottom of the cell, in concert with the increase in PI 3-kinase activity at the top, exacerbates the initial decrease in fluorescence at the center of the contact area.

Fluorescence measurements can be used to identify bounds on the relative rates of 3′ phosphoinositide consumption versus diffusion and other dimensionless groups

The constraints-based approach presented in Fig. 5 also delineates limiting behavior, which is important for the analysis of experiments. For example, there exists a minimum p_{ss} required to achieve a given $f_{min}(0)$, evaluated in the limit of very large κ or μ (the $\mu = 5$ curves in Fig. 5, *a* and *b*, suffice here). In this limit, it is ensured that the free lipid is always in great excess over bound probe. For a given $f_{min}(0)$, there also exists an upper limit on p_{ss}, evaluated in the limit of vanishing κ. In this limit, the probe affinity is high enough that the amount of bound probe is approximately equal to the total number of 3′ PI or probe molecules, whichever is smaller. An intermediate condition, then, would be a parameter set for which half of the lipid is bound by probe at steady state, satisfied by $\kappa = 1 - p_{ss}$ (marked by the *black curves* in Fig. 5, *a* and *b*). The corresponding values of x_0 in those limits can also be discerned from Fig. 5, *a* and *b*. One may thus identify those parameter sets that yield certain values of $f_{min}(0)$ as well as f_0, $\bar{f}_{ss}$, and $f_{ss}(0)$, e.g., as observed in an experiment. Taken together, the large μ limit, the low κ limit, and the assumption that ν is no greater than x_0 define useful parameter ranges, as shown in Table 2 with $f_0 = 0.40$, $\bar{f}_{ss} = 2.00$, $f_{ss}(0) = 1.18$, and $f_{min}(0) = 0.00$.

Indeed, the limits on *Da* in particular can be relatively narrow, as explored further in Fig. 6 *a* for a wide range of $f_{min}(0)$ values. With $f_{min}(0) = 0.00$, the upper and lower limits on *Da* are 2.81 and 3.52, respectively (Table 2), a difference of 22%. As shown in Fig. 6 *a*, it is often the case that one or more of the limiting cases is unable to yield the specified fluorescence values; the inclusion of the intermediate case, $\kappa = 1 - p_{ss}$, is therefore a compromise to define more of the allowable parameter space. Thus, with the fluorescence values given, it is apparent that the range of *Da* values would be even narrower for $f_{min}(0)$ values above or below 0.00 (Fig. 6 *a*). Fig. 6 *b* shows the corresponding limits on the value of σ. Of note here is the insensitivity of $f_{min}(0)$ to the value of σ when the dip in fluorescence is relatively shallow, which can lead to arbitrarily high estimates of σ for certain values of $f_{min}(0)$.

With the four values $f_0, \bar{f}_{ss}, f_{ss}(0)$, and $f_{min}(0)$ specified, is it possible to distinguish different parameter sets based on other aspects of the association and/or dissociation kinetics? This is addressed in Fig. 7 by comparing the kinetics simulated with the five sets of parameters listed in Table 2. It is apparent that, with the data features fixed in this manner, there is relatively little difference among the association time courses for these parameter sets. However, in the dissociation kinetics there is significant variation in the onset of fluorescence decay. The decay is delayed when most of the probe is bound, yet free 3′ PI molecules are abundant, and the deviation from single exponential decay can be assessed using the ratio of the rate of decrease in p over its value, $(-dp/d\tau)/p = -d(\ln p)/dt$; with pure single exponential decay, this quantity is equal to one. In the initial decay from the steady state, we find that

$$-\left.\frac{d(\ln p)}{d\tau}\right|_{\tau=0} = \frac{1+\kappa(1-p_{ss})^{-1}}{1+\kappa(1-p_{ss})^{-2}}. \quad (5)$$

For comparison, the values of $-d(\ln p)/dt$ at the beginning of the dissociation runs for parameter sets 1–5 in Fig. 7 are 0.48, 0.50, 0.85, 0.37, and 0.24 respectively.

TABLE 2 Parameter sets that yield $f_0 = 0.40$, $\bar{f}_{ss}=2.00$, $f_{ss}(0) = 1.18$, and $f_{min}(0) = 0.00$

	Set 1 $\nu = 0, \mu = 5$	Set 2 $\nu = 0, \kappa = 1 - p_{ss}$	Set 3 $\nu = 0, \kappa = 10^{-3}$	Set 4 $\nu = x_0, \mu = 5$	Set 5 $\nu = x_0, \kappa = 1 - p_{ss}$	Set 6 $\nu = x_0, \kappa = 10^{-3}$
p_{ss}	**0.533**	0.664	**0.927**	0.641	0.861	None*
Da	3.36	3.15	**2.81**	**3.52**	3.29	
σ	**22.6**	18.7	**14.2**	19.3	15.1	
x_0	0.0403	0.0524	**0.0760**	**0.0332**	0.0453	

Parameter extremes for these fluorescence characteristics are highlighted in bold.
*The specified fluorescence characteristics cannot be achieved with these constraints.

DISCUSSION

Live-cell fluorescence experiments have yielded significant insights into the regulation of intracellular signaling events (Weijer, 2003). Unlike biochemical methods, the use of specific fluorescent probes gives us direct spatial information, but a shortcoming of this approach is that image analysis introduces a significant bottleneck. The fact that cells, as individuals, behave in various ways means that a large and tedious effort is generally required to characterize spatially regulated signaling processes, and a compromise must be made between spatial resolution and the number of cells observed in each experiment (Teruel and Meyer, 2002). We have formulated a generalized mathematical model that can be directly compared with TIRF microscopy experiments, and a methodology was devised for extracting ranges of dimensionless parameter values from only four well-defined fluorescence intensity measurements: the initial fluorescence, the minimum fluorescence at the center of the contact area, and two features of the steady-state fluorescence profile. From an image analysis point of view, this approach is simple enough that it could be automated, and thus the characterization of individual cell parameters might be accelerated.

In terms of the 3′ PI dynamics, the key dimensionless group is Da, which relates the effective rates of 3′ PI turnover and diffusion. We have demonstrated that this parameter can be estimated with adequate precision, with typical differences between the minimum and maximum Da values of ~20% or less. Our robust parameter estimation method achieves this precision without regression fitting, although it would be necessary then to fit or otherwise compare points in time to obtain the dimensional values of the effective 3′ PI diffusion coefficient, D, and turnover rate constant, k. Indeed, this is the approach taken as this methodology was applied to the analysis of actual experiments (described in the companion article that follows).

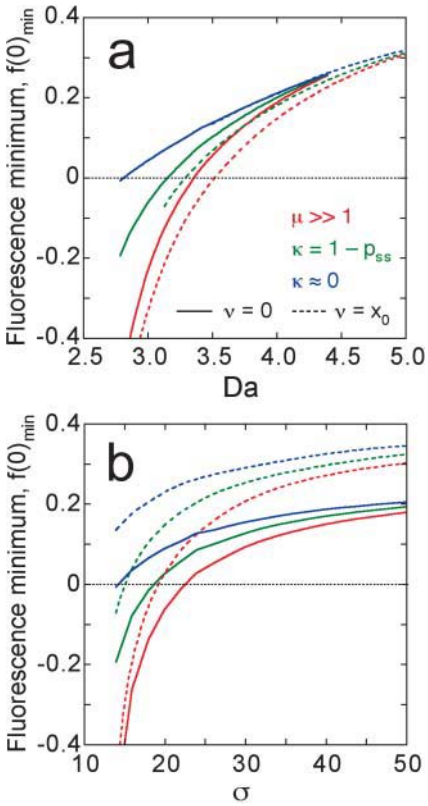

FIGURE 6 Identification of upper and lower bounds on the dimensionless parameters. Relationships between the value of Da (a) or σ (b) and the $f_{min}(0)$ achieved, with other parameters chosen to set $f_0 = 0.40$, $\bar{f}_{ss} = 2.00$, and $f_{ss}(0) = 1.18$ as in Fig. 5. Solid lines are with $\nu = 0$; dashed lines are with $\nu = x_0$. Colors signify the high-affinity limit ($\kappa = 10^{-3}$; *blue*), the excess-lipid limit ($\mu = 5$; *red*), or the intermediate condition ($\kappa = 1 - p_{ss}$; *green*). The global Da and σ minima (evaluated at $\nu = 0, p_{ss} = 1$) are 2.73 and 13.4, respectively.

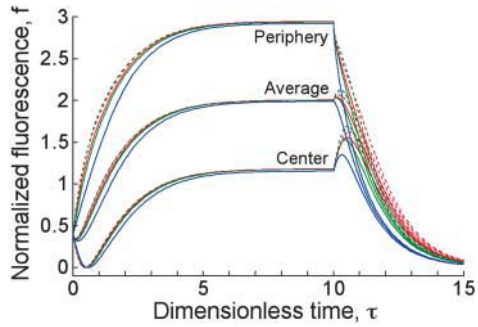

FIGURE 7 Simulated association-dissociation kinetics with extreme parameter sets. The five extreme parameter sets listed in Table 2, satisfying $f_0 = 0.40, \bar{f}_{ss} = 2.00, f_{ss}(0) = 1.18$, and $f_{min}(0) = 0.00$ in various limits, were used to simulate association-dissociation experiments in dimensionless time. Solid lines are with $\nu = 0$; dashed lines are with $\nu = x_0$. Colors signify the high-affinity limit ($\kappa = 10^{-3}$; *blue*), the excess-lipid limit ($\mu = 5$; *red*), or the intermediate condition ($\kappa = 1 - p_{ss}$; *green*).

A simplification in the model was the choice of an idealized yet reasonable cellular geometry, in which the contact area is circular. A square contact area (which has the same area/perimeter ratio as a circle inscribed within it) yielded almost identical results, whereas rectangular areas with large aspect ratios require a Da value almost 2 times lower to achieve a similar profile (results not shown). As cells are analyzed, then, the variability of the contact area geometry should be acknowledged or accounted for. The shape of the top domain is less critical, however, because the 3′ PI distribution in the nonadherent membrane simply provides the boundary flux into the contact area. The major determinant of the flux is the relative surface area of the top membrane domain; i.e., the top domain contains two-thirds of the membrane area for a hemispherical cell, compared with one-half for a ''pancake'' morphology. Such differences can be artificially offset by adjusting the value of the TIRF gain parameter, σ, as shown for changes in the ratio of diffusion coefficients, γ (Fig. 4 *c*).

Another issue related to the morphology of fibroblasts and other anchorage-dependent cells is the presence of thin structures, such as filopodia and the trailing uropod, radiating from the adhesion zone, which are expected to exhibit 3′ PI profiles that are different from the body of the contact area. In such a structure, 3′ PIs are expected to diffuse across its width before significant turnover can occur; thus, for the same rate of 3′ PI production in the nonadherent membrane, the thinner structures would appear brighter when excited by TIRF. This is indeed what has been generally observed in filopodia-like structures, but not uropods, of our cells (Haugh et al., 2000). The question thus arises whether or not the 3′ PI production rate is differentially regulated in such structures so as to further enhance or abrogate the accumulation of 3′ PIs. We are currently using the model to address these possibilities. In any case, the dependence of the 3′ PI level on cell morphology is a direct outcome of the restriction of PDGF-stimulated 3′ PI production to the nonadherent portion of the cell, and it is intriguing that 3′ PIs in turn control cell morphology through the regulation of cell spreading and motility.

A second simplification in our analysis was the assumption that PDGF stimulation induces step changes in the PI 3-kinase activities associated with the two domains, which is justified when the concentration of PDGF is sufficiently high. This assumption is not necessary, however, because the generalized model can accommodate any kinetics. Indeed, we are currently working to incorporate a recently developed kinetic model of PDGF receptor phosphorylation and PI 3-kinase recruitment (Park et al., 2003). Although the inclusion of receptor-mediated processes comes with an increase in the number of model parameters, it would allow the application of the model to a much wider range of experimental conditions. Clearly, adding complexity to any model of intracellular signaling in a judicious manner requires a significant amount of quantitative experimental data, and in this respect fluorescence imaging of individual cells and biochemical measurements of cell populations are expected to complement each other.

APPENDIX A: UNIFORM STIMULATION MODEL SOLUTION AND CALCULATIONS

Solution of the partial differential equations

From Eqs. 1–3, the 3′ PI densities in the two domains are found using the finite Fourier transform method (Deen, 1998):

$$\begin{aligned} x_b(\rho,\tau) &= e^{-\tau}\int_0^\tau \upsilon_b e^{\tau}\,d\tau \\ &\quad + 2\sum_{n=0}^{\infty}\Phi_n e^{-b_n\tau}\left[\int_0^1 x_b(\rho,0)\Phi_n\rho\,d\rho + \int_0^\tau g e^{b_n\tau}\,d\tau\right] \\ &\quad \Phi_n(\rho)\equiv J_0(\lambda_n\rho)/J_0(\lambda_n);\quad J_1(\lambda_n)=0; \\ &\quad b_n\equiv 1+\lambda_n^2/Da \end{aligned} \tag{A1}$$

$$\begin{aligned} x_t(\eta,\tau) &= \alpha e^{-\alpha\tau}\int_0^\tau \upsilon_t e^{\alpha\tau}\,d\tau \\ &\quad + \sum_{n=0}^{\infty}\Psi_n e^{-a_n\tau}\left[\int_0^1 x_t(\eta,0)\Psi_n\,d\eta - \Psi_n(0)\int_0^\tau g e^{a_n\tau}\,d\tau\right] \\ &\quad \Psi_n(\eta)\equiv (4n+1)^{1/2}P_{2n}(\eta); \\ &\quad a_n\equiv \alpha + 2n(2n+1)\gamma/Da, \end{aligned} \tag{A2}$$

where J_m and P_m are Bessel functions and Legendre polynomials of order m, respectively, and the boundary gradient function g is defined as

$$g(\tau)=\frac{1}{Da}\frac{\partial x_b(1,\tau)}{\partial\rho}=\frac{\gamma}{Da}\frac{\partial x_t(0,\tau)}{\partial\eta}. \tag{A3}$$

Calculated average and steady-state 3′ PI concentrations

The average 3′ PI concentration in each domain is found using surface integrals. Only the leading terms in the infinite series contribute:

$$\bar{x}_b(\tau)\equiv 2\int_0^1 x_b(\rho,\tau)\rho d\rho = e^{-\tau}\left[\bar{x}_b(0)+\int_0^\tau \upsilon_b e^{\tau}d\tau + 2\int_0^\tau g e^{\tau}d\tau\right]; \tag{A4}$$

$$\bar{x}_t(\tau)\equiv \int_0^1 x_t(\eta,t)d\eta = e^{-\alpha\tau}\left[\bar{x}_t(0)+\alpha\int_0^\tau \upsilon_t e^{\alpha\tau}d\tau - \int_0^\tau g e^{\alpha\tau}d\tau\right]. \tag{A5}$$

These quantities are used to calculate the total number of 3′ PI molecules in the cell, which is proportional to

$$x_{Tot}(\tau)\equiv 2\bar{x}_t(\tau)+\bar{x}_b(\tau). \tag{A6}$$

Provided that a nonzero steady state is achieved, one may define X^* such that $\upsilon_{t,ss}=1$, and the boundary gradient g_{ss} and the dimensionless steady-state 3′ PI distribution in the bottom domain are readily derived:

$$g_{ss} = (1-\nu)\left[Da^{1/2}\frac{I_0(Da^{1/2})}{I_1(Da^{1/2})} + \sum_{n=0}^{\infty}\frac{\Psi_n^2(0)}{a_n}\right]^{-1}$$

$$x_{b,ss}(\rho) = \nu + g_{ss}\frac{Da^{1/2}I_0(Da^{1/2}\rho)}{I_1(Da^{1/2})}; \quad \nu \equiv \frac{V_{b,ss}}{V_{t,ss}}\frac{k_t}{k_b}, \qquad \text{(A7)}$$

where I_m are modified Bessel functions of order m. At steady state, the quantity x_{Tot} from Eq. A6 reduces to

$$x_{Tot,ss} = 2 + \nu - 2(\alpha^{-1} - 1)g_{ss}. \qquad \text{(A8)}$$

As described in the Results section, convenient steady-state metrics are the quantities $f_{ss}(0)/\bar{f}_{ss}$ and $\bar{f}_{ss}/p_{ss}$, given by

$$\frac{f_{ss}(0)}{\bar{f}_{ss}} = \frac{\sigma\left[\nu + Da^{1/2}g_{ss}/I_1(Da^{1/2})\right] - x_{Tot,ss}}{\sigma(\nu + 2g_{ss}) - x_{Tot,ss}}; \qquad \text{(A9)}$$

$$\bar{f}_{ss}/p_{ss} = \sigma(\nu + 2g_{ss})/x_{Tot,ss} - 1. \qquad \text{(A10)}$$

Computation of 3′ PI density profiles

The quantities $x_b(\rho,\tau)$, $x_t(\eta,\tau)$, $\bar{x}_b(\tau)$, and $\bar{x}_t(\tau)$ were computed using subroutines composed in Fortran 90 (available upon request). Briefly, each spatial domain is split into 50 equal segments in ρ or η, and the initial conditions $x_b(\rho,0)$ and $x_t(\eta,0)$ are read from data files. Before stimulation, the initial conditions $x_b(\rho,0) = x_t(\eta,0) = x_0$ (constant) were generally assumed; for PI 3-kinase inhibition, the steady-state distributions immediately before inhibitor addition are used to reinitialize the simulation. The infinite series in Eqs. A1 and A2 are truncated at 2000 terms, and the integrals containing $x_b(\rho,0)$ and $x_t(\eta,0)$ are evaluated numerically. Dimensionless time τ is stepped 1000 times for each of the intervals 10^{-5}, 10^{-4}, 10^{-3}, and 10^{-2}, for a total time τ of 11.11. At each time step, the boundary gradient function $g(\tau)$ and the associated integrals are estimated as described below. It was confirmed that decreasing the time steps by a factor of 10, or increasing the number of terms in the infinite series by twofold, did not significantly affect the program output at a resolution of 0.01 in τ.

The function $g(\tau)$ is found by matching $x_b(1,\tau)$ and $x_t(0,\tau)$ at the perimeter. Its evaluation is aided by the approximation that it is linear over a sufficiently small interval, i.e.,

$$\int_{y_1}^{y_2} g(y)e^y dy \approx e^{y_2}g(y_2) - e^{y_1}g(y_1) - \frac{e^{y_2} - e^{y_1}}{y_2 - y_1}[g(y_2) - g(y_1)]. \qquad \text{(A11)}$$

Our new method for estimating $g(\tau)$ involves a linear interpolation, incorporating Eqs. A1, A2, and A11:

$$g(\tau) \approx \frac{1}{2}[g(\tau - \Delta\tau) + g(\tau + \Delta\tau)]$$

$$\approx \frac{h(\tau) - \sum_{n=0}^{\infty}\left[\frac{\Phi_n^2(0)}{a_n}\Omega_{a_n}(\tau, 2\Delta\tau) + \frac{2}{b_n}\Omega_{b_n}(\tau, 2\Delta\tau)\right]}{\sum_{n=0}^{\infty}\left[\frac{\Phi_n^2(0)}{a_n}\left(1 - \frac{1 - e^{-2a_n\Delta\tau}}{2a_n\Delta\tau}\right) + \frac{2}{b_n}\left(1 - \frac{1 - e^{-2b_n\Delta\tau}}{2b_n\Delta\tau}\right)\right]}$$

$$h(\tau) \equiv \alpha e^{-\alpha\tau}\int_0^{\tau} v_t e^{\alpha\tau}\, d\tau - e^{-\tau}\int_0^{\tau} v_b e^{\tau}\, d\tau + \sum_{n=0}^{\infty}\left[\Psi_n(0)e^{-a_n\tau}\int_0^1 x_{t,0}\Psi_n\, d\eta - 2e^{-b_n\tau}\int_0^1 x_{b,0}\Phi_n\rho\, d\rho\right], \qquad \text{(A12)}$$

subject to the recursion formula

$$\Omega_c(y,\Delta y) = e^{-c\Delta y}\Omega_c(y - \Delta y, \Delta y) + \frac{(1 - e^{-c\Delta y})^2}{c\Delta y}g(y - \Delta y)$$

$$\Omega_c(0,\Delta y) = 0. \qquad \text{(A13)}$$

APPENDIX B: FROM LIPID DENSITY PROFILES TO FLUORESCENCE PROFILES

The fluorescence intensity, F, is normalized to give the scaled quantity, f, where F_{cyt} is the intensity observed when all of the fluorescent probe is in the cytosol:

$$f(\rho,\tau) \equiv \frac{F(\rho,\tau) - F_{cyt}}{F_{cyt}}. \qquad \text{(B1)}$$

The fluorescence F is the sum of two contributions, from probe molecules in the cytosol and from those bound to the membrane contact area. We assume that the probe diffuses rapidly within the cytosol. Taking C to be the free concentration of the probe everywhere in the cytosol, and noting that the energy of an evanescent wave decays exponentially with distance, the cytosolic contribution is given by

$$F_1 = aC(\tau)\int_0^{\infty} e^{-z/d_{cell}}dz = a\, d_{cell}C(\tau), \qquad \text{(B2)}$$

where a is the fluorescence per unit GFP-AktPH and d_{cell} is the space constant for the penetration of the evanescent wave (~100 nm). Let $p(\tau)$ be the fraction of the probe that is bound to 3′ PIs in both the bottom and top membrane domains; assuming pseudo-equilibrium between bound and unbound probe, and accounting for the fact that probe binding depletes both the cytosolic probe and the number of free 3′ PI molecules, p is given by

$$p(\tau) = 1 - V_{cyt}C(\tau)/P_{Tot} = \frac{C(\tau)}{K_D}\left[\frac{A_cX^*x_{Tot}(\tau)}{P_{Tot}} - p(\tau)\right], \qquad \text{(B3)}$$

where P_{Tot} is the total number of probe molecules in the cell, V_{cyt} is volume of the cytosol, K_D is the dissociation constant of the probe-3′ PI interaction, and A_c is the surface area of the membrane contact region. With x_{Tot} defined as in Eq. A6, the quantity $A_cX^*x_{Tot}$ is the total number of 3′ PI molecules in the cell. Pseudo-equilibrium also holds at every point in the contact area; defining $PX(\rho,\tau)$ as the density of probe-3′ PI complexes at a given location,

$$PX(\rho,\tau) = \frac{C(\tau)}{K_D}[X^*x_b(\rho,\tau) - PX(\rho,\tau)]. \qquad \text{(B4)}$$

Combining Eqs. B3 and B4,

$$PX(\rho,\tau) = \frac{x_b(\rho,\tau)}{x_{Tot}(\tau)}\frac{P_{Tot}}{A_c}p(\tau). \qquad \text{(B5)}$$

Now suppose that the bound probe is confined to a small distance δ adjacent to the plasma membrane (<10 nm). The effective concentration of the bound probe at a particular contact area position is thus PX/δ, and assuming $\delta/d_{cell} \ll 1$, its fluorescence contribution is

$$F_2 = a(PX/\delta)\int_0^{\delta} e^{-z/d_{cell}}\, dz \approx aPX(\rho,\tau). \qquad \text{(B6)}$$

The total fluorescence, F, is found by summing F_1 and F_2 from Eqs. B2 and B6. Finally, noting that

$$F_{\mathrm{cyt}} = a\frac{P_{\mathrm{Tot}}}{V_{\mathrm{cyt}}}d_{\mathrm{cell}}, \tag{B7}$$

and incorporating Eqs. B1, B3, and B5, we obtain the normalized fluorescence, $f(\rho,\tau)$:

$$f(\rho,\tau) = \left[\frac{\sigma x_{\mathrm{b}}(\rho,\tau)}{x_{\mathrm{Tot}}(\tau)} - 1\right]p(\tau); \quad \sigma \equiv \frac{V_{\mathrm{cyt}}}{A_{\mathrm{c}}d_{\mathrm{cell}}}. \tag{B8}$$

From the relations given in Eq. B3, $C(\tau)$ can be eliminated and $p(\tau)$ expressed in terms of $x_{\mathrm{Tot}}(\tau)$ and constants:

$$p(\tau) = \frac{1+\kappa+\mu x_{\mathrm{Tot}} - \left[(1+\kappa+\mu x_{\mathrm{Tot}})^2 - 4\mu x_{\mathrm{Tot}}\right]^{1/2}}{2}$$
$$\kappa \equiv K_{\mathrm{D}}V_{\mathrm{cyt}}/P_{\mathrm{Tot}}; \quad \mu \equiv A_{\mathrm{c}}X^*/P_{\mathrm{Tot}}. \tag{B9}$$

This work was supported by the Whitaker Foundation (RG-01-0150) and from an award to J.M.H. from the Henry & Camille Dreyfus Foundation. I.C.S. was also supported by a Graduate Assistance in Areas of National Need Biotechnology Fellowship from the U.S. Department of Education.

REFERENCES

Asthagiri, A. R., and D. A. Lauffenburger. 2000. Bioengineering models of cell signaling. *Annu. Rev. Biomed. Eng.* 2:31–53.

Axelrod, D. 2001. Total internal reflection fluorescence microscopy in cell biology. *Traffic.* 2:764–774.

Botelho, R. J., M. Teruel, R. Dierckman, R. Anderson, A. Wells, J. D. York, T. Meyer, and S. Grinstein. 2000. Localized biphasic changes in phosphatidylinositol-4,5-bisphosphate at sites of phagocytosis. *J. Cell Biol.* 151:1353–1367.

Deen, W. M. 1998. Analysis of Transport Phenomena. Oxford University Press.

Fink, C. C., B. Slepchenko, I. I. Moraru, J. Schaff, J. Watras, and L. M. Loew. 1999. Morphological control of inositol-1,4,5-trisphosphate-dependent signals. *J. Cell Biol.* 147:929–935.

Harriague, J., and G. Bismuth. 2002. Imaging antigen-induced PI3K activation in T cells. *Nat. Immunol.* 3:1090–1096.

Haugh, J. M. 2002. A unified model for signal transduction reactions in cellular membranes. *Biophys. J.* 82:591–604.

Haugh, J. M., F. Codazzi, M. Teruel, and T. Meyer. 2000. Spatial sensing in fibroblasts mediated by 3′ phosphoinositides. *J. Cell Biol.* 151:1269–1279.

Haugh, J. M., and D. A. Lauffenburger. 1998. Analysis of receptor internalization as a mechanism for modulating signal transduction. *J. Theor. Biol.* 195:187–218.

Hunter, T. 2000. Signaling—2000 and beyond. *Cell.* 100:113–127.

Levchenko, A., and P. A. Iglesias. 2002. Models of eukaryotic gradient sensing: application to chemotaxis of amoebae and neutrophils. *Biophys. J.* 82:50–63.

Marshall, J. G., J. W. Booth, V. Stambolic, T. Mak, T. Balla, A. D. Schreiber, T. Meyer, and S. Grinstein. 2001. Restricted accumulation of phosphatidylinositol 3-kinase products in a plasmalemmal subdomain during Fc gamma receptor-mediated phagocytosis. *J. Cell Biol.* 153: 1369–1380.

Narang, A., K. K. Subramanian, and D. A. Lauffenburger. 2001. A mathematical model for chemoattractant gradient sensing based on receptor-regulated membrane phospholipid signaling dynamics. *Ann. Biomed. Eng.* 29:677–691.

Parent, C. A., and P. N. Devreotes. 1999. A cell's sense of direction. *Science.* 284:765–770.

Park, C. S., I. C. Schneider, and J. M. Haugh. 2003. Kinetic analysis of platelet-derived growth factor receptor/phosphoinositide 3-kinase/Akt signaling in fibroblasts. *J. Biol. Chem.* 278:37064–37072.

Postma, M., and P. J. M. Van Haastert. 2001. A diffusion-translocation model for gradient sensing by chemotactic cells. *Biophys. J.* 81:1314–1323.

Pribyl, M., C. B. Muratov, and S. Y. Shvartsman. 2003. Long-range signal transmission in autocrine relays. *Biophys. J.* 84:883–896.

Rameh, L. E., and L. C. Cantley. 1999. The role of phosphoinositide 3-kinase lipid products in cell function. *J. Biol. Chem.* 274:8347–8350.

Schaff, J., C. C. Fink, B. Slepchenko, J. H. Carson, and L. M. Loew. 1997. A general computational framework for modeling cellular structure and function. *Biophys. J.* 73:1135–1146.

Shea, L. D., G. M. Omann, and J. J. Linderman. 1997. Calculation of diffusion-limited kinetics for the reactions in collision coupling and receptor cross-linking. *Biophys. J.* 73:2949–2959.

Steyer, J. A., and W. Almers. 2001. A real-time view of life within 100 nm of the plasma membrane. *Nat. Rev. Mol. Cell Biol.* 2:268–275.

Swaminathan, R., C. P. Hoang, and A. S. Verkman. 1997. Photobleaching recovery and anisotropy decay of green fluorescent protein GFP-S65T in solution and cells: cytoplasmic viscosity probed by green fluorescent protein translational and rotational diffusion. *Biophys. J.* 72:1900–1907.

Teruel, M. N., and T. Meyer. 2002. Parallel single-cell monitoring of receptor-triggered membrane translocation of a calcium-sensing protein module. *Science.* 295:1910–1912.

Toomre, D., and D. J. Manstein. 2001. Lighting up the cell surface with evanescent wave microscopy. *Trends Cell Biol.* 11:298–303.

Vanhaesebroeck, B., S. J. Leevers, K. Ahmadi, J. Timms, R. Katso, P. C. Driscoll, R. Woscholski, P. J. Parker, and M. D. Waterfield. 2001. Synthesis and function of 3-phosphorylated inositol lipids. *Annu. Rev. Biochem.* 70:535–602.

Wang, F., P. Herzmark, O. D. Weiner, S. Srinivasan, G. Servant, and H. R. Bourne. 2002. Lipid products of PI(3)Ks maintain persistent cell polarity and directed motility in neutrophils. *Nat. Cell Biol.* 4:513–518.

Weijer, C. J. 2003. Visualizing signals moving in cells. *Science.* 300:96–100.

Weiner, O. D. 2002. Regulation of cell polarity during eukaryotic chemotaxis: the chemotactic compass. *Curr. Opin. Cell Biol.* 14:196–202.

Weng, G., U. S. Bhalla, and R. Iyengar. 1999. Complexity in biological signaling systems. *Science.* 284:92–96.

Xu, C., J. Watras, and L. M. Loew. 2003. Kinetic analysis of receptor-activated phosphoinositide turnover. *J. Cell Biol.* 161:779–791.

Yokoe, H., and T. Meyer. 1996. Spatial dynamics of GFP-tagged proteins investigated by local fluorescence enhancement. *Nat. Biotechnol.* 14: 1252–1256.